Article

Preparation of Li_2S-AlI_3-LiI Composite Solid Electrolyte and Its Application in All-Solid-State Li-S Battery

Tran Anh Tu [1,2], Nguyen Huu Huy Phuc [1,2,*], Luong Thi Quynh Anh [1,2] and Tran Viet Toan [1,2]

1 Faculty of Materials Technology, Ho Chi Minh City University of Technology (HCMUT), 268 Ly Thuong Kiet Str., Dist. 10, Ho Chi Minh City 70000, Vietnam; attran@hcmut.edu.vn (T.A.T.); ltqanh@hcmut.edu.vn (L.T.Q.A.); tvtoan@hcmut.edu.vn (T.V.T.)
2 Vietnam National University Ho Chi Minh City, Linh Trung Ward, Thu Duc Dist., Ho Chi Minh City 70000, Vietnam
* Correspondence: nhhphuc@hcmut.edu.vn

Abstract: Novel $(80Li_2S - 20AlI_3) \cdot yLiI$ composite solid electrolytes (y = 5, 10, 15) were prepared by mechannochemical synthesis. XRD results showed that the pattern of $80Li_2S - 20AlI_3$ was similar to that of AlI_3, which means that Li_2S was dissolved in AlI_3 matrix during preparation. This structure was still maintained after LiI addition. The current measured at constant applied DC voltage indicated that $(80Li_2S - 20AlI_3) \cdot yLiI$ composites are intrinsically pure Li-ion conductors. The ionic conductivity at 25 °C of y = 10 was about 2.3×10^{-4} Scm^{-1}, which was about three times higher than that of y = 0. The conductivity of y = 10 increased 20 times to 2.2×10^{-3} Scm^{-1} at 70 °C. These values were highest among those observed from Li_2S-based materials. It was revealed that Li-ion moves in $80Li_2S - 20AlI_3$ by a hoping mechanism, while the lattice dipoles are the origin of Li-ion movement in $(80Li_2S - 20AlI_3) \cdot yLiI$. The polarization measurements using $LiI90 (80Li_2S - 20AlI_3) \cdot 10LiI|Li$ and $LiI|Li_6PS_5Cl|90 (80Li_2S - 20AlI_3) \cdot 10LiI|Li_6PS_5Cl|Li$ cells proved that $90 (80Li_2S - 20AlI_3) \cdot 10LiI$ reacts with Li metal, but it is relatively stable at a low voltage. Sample y = 10 was also employed as a solid electrolyte in the positive electrode of a solid-state Li-S battery to study its stability in the voltage range of the positive electrode. CuS and $Li_{4.4}Si$ were the electrode-active materials. The cell was cycled in CC-CV mode at 1.0 mA cm^{-2} (CC) with a cut-off voltage of 1.0–2.3 V. The cell delivered a stable capacity of about 400 mAh g^{-1}_{CuS} after 40 cycles.

Keywords: Li_2S conductivity; Li-S battery; solid-state battery; complex impedance spectroscopy

1. Introduction

Sulfide-based solid electrolytes (SEs) are one of the candidates for all-solid-state (ASS) Li-ion batteries due to their high ionic conductivity at room temperature and suitable mechanical properties [1–3]. $Li_7P_3S_{11}$, $Li_{10}GeP_2S_{12}$, and $Li_{5.5}PS_{4.5}Cl_{1.5}$ exhibited ionic conductivity higher than 10^{-2} Scm^{-1} at 25 °C [4–6]. Sulfide-based solid electrolytes can be prepared using different methods: solid-state reaction at high temperature, mechanosynthesis, and liquid phase synthesis [7–9]. Until now, most of the reported sulfide-based solid electrolytes have belonged to Li_2S-P_2S_5-LiX (X = halogen) groups; therefore, the search for sulfide-based electrolytes that do not contain P_2S_5 is an interesting research direction.

The glass and glass-ceramic electrolytes of the $(100 - x)Li_2S$-xAl_2S_3 group were synthesized using planetary ball milling and thoroughly studied [10]. Amorphous $60Li_2S \cdot 40AlS_{1.5}$ was obtained with a milling speed of 230 rpm, while glass-ceramic containing Li_5AlS_4 crystal was directly obtained with a milling speed of 510 rpm for 2 h. The highest conductivity of 3.4×10^{-5} Scm^{-1} at 25 °C was obtained for the $60Li_2S \cdot 40AlS_{1.5}$ amorphous electrolytes. Li_2S-SiS_2 and Li_3PO_4-Li_2S-SiS_2 glassy SEs were also prepared by the melt-quenching method, and their ionic conductivities and electrochemical properties were investigated [11,12]. The highest conductivity, of about 7.6×10^{-4} Scm^{-1} at 25 °C, was obtained in those systems. The solid-state cell using graphite as active material and

0.03Li$_3$PO$_4$-0.58Li$_2$S-0.39SiS$_2$ as solid electrolyte showed good cycle performance. On the other hand, Li$_2$S-SiS$_2$ amorphous materials were also prepared by mechanochemical synthesis and showed the highest conductivity of about 3.4 × 10^{-4} Scm^{-1} at 25 °C [13].

Li$_2$S has been intensively used as positive electrode material in the Li-S battery because its usage enables the employment of graphite or silicon in the negative electrode. However, Li$_2$S is a natural insulator to both electrons and ions; much effort has been made to increase the electron and ionic conductivity of Li$_2$S. Fabricating composites with carbonaceous materials, such as graphene, carbon nanotubes, or carbon nanofibers, will increase the electronic conductivity of Li$_2$S [14–17]. On the other hand, many other methods for increasing the ionic conductivity of Li$_2$S have been reported so far. Composite nanoparticles with Li$_2$S as the core and Li$_3$PS$_4$ as the shell exhibit ionic conductivity of about 10^{-7} Scm^{-1} at 25 °C, which is 10^4 times higher than that of Li$_2$S nanoparticles [18]. The ionic conductivity of Li$_2$S- Li$_3$PS$_4$ reaches 10^{-4} Scm^{-1} at 25 °C in another report [19]. The ionic conductivity of Li$_2$S-LiX solid solution (X = halogen) is about 10^{-6} Scm^{-1}, which is about 10^2 times higher than that of Li$_2$S [20]. Solid solutions of Li$_2$S and multivalence cation sulfides, Li$_{2-2x}$Mg$_x$S (0.05 ≤ x ≤ 0.2) and Li$_{2-3x}$Al$_x$S (0 ≤ x ≤ 0.1667), also show improved ionic conductivity compared with Li$_2$S [21,22]. The ionic conductivity of 80Li$_2$S·20AlI$_3$ even reaches 6.0 × 10^{-5} Scm^{-1} at 25 °C [23]. In the same study, 99.5Li$_2$S·0.5AlI$_3$ acted as both SE and active material in an all-solid-state battery. In addition, antiperovskite-like type Li$_3$SI had an ionic conductivity of 2.2 × 10^{-5} Scm^{-1} at 25 °C and was employed as SE in the ASS Li-ion battery [24]. It should be noted that the application of Li$_2$S-based as SE in the ASS battery is very rare due to its low ionic conductivity.

In this study, a series of (100 − x)Li$_2$S-xAlI$_3$ and (80Li$_2$S − 20AlI$_3$)·yLiI composite solid electrolytes (y = 5, 10, 15) were prepared by mechanochemical synthesis and investigated using XRD and AC impedance spectroscopy. The ionic conductivity at 25 °C (80Li$_2$S − 20AlI$_3$)·yLiI (y = 5, 10, 15) is higher than that of 80Li$_2$S·20AlI$_3$ and Li$_3$SI because LiI addition reduces the resistance at the grain boundary and interface; to the best of our knowledge, such effects of LiI have not been reported before. Among them, sample (80Li$_2$S − 20AlI$_3$)·10LiI has the highest ionic conductivity, which is about 2.3 × 10^{-4} Scm^{-1} at 25 °C. In addition, the complex conductivity suggested the formation of a composite consisting of 80Li$_2$S − 20AlI$_3$ and LiI rather than a solid solution due to the existence of two slopes in the low-frequency region. The use of complex conductivity to differentiate solid solutions from composites has also not been noted before. The electronic conductivity of (80Li$_2$S − 20AlI$_3$)·10LiI is about 1.1 × 10^{-8} Scm^{-1}; therefore, (80Li$_2$S − 20AlI$_3$)·10LiI is a pure Li-ion conductor. The solid-state cell, which employs CuS as active material and (80Li$_2$S − 20AlI$_3$)·10LiI as solid electrolyte, delivers a stable capacity after 40 cycles.

2. Experimental

Li$_2$S (99.9%), LiCl (99.9%), AlI$_3$ (99.9%), Si (99.99%), Li metal (99.99%), CuS (99.9%), and LiI (99.9%) were purchased from Sigma. P$_2$S$_5$ (99%) was purchased from Merck Group. All chemicals were used without purification.

(100 − x)Li$_2$S-xAlI$_3$ and (80Li$_2$S − 20AlI$_3$)·yLiI composite solid electrolytes (y = 5, 10, 15) were prepared via planetary ball milling using the same conditions as reported previously [23]. For a typical batch, Li$_2$S, AlI$_3$, and LiI were manually mixed for 10 min prior to introduction into 45 mL zirconia pots with zirconia balls (10 mm, 15 balls). The pots were then rotated at 500 rpm for 12 h using a Pulverisette 7 (Fritsch). The obtained samples were recovered and used without any further heat treatment. Li$_{4.4}$Si was prepared using the procedure reported by Tamori et al. [25]. A total of 0.7814 g Li and 0.7186 g Si (Li:Si = 4.4:1.0 mole ratio) was manually mixed using an agate mortar for about 15 min; the obtained mixture was then introduced into 45 mL zirconia pots with zirconia balls (4 mm, 10 balls). The pots were then rotated at 200 rpm. For one cycle, 10 min milling time and 5 min resting time was employed to avoid the sample from temperature increasing. Li$_{4.4}$Si was recovered after 50 h of milling time. Li$_6$PS$_5$Cl was prepared using the same method. In a typical batch, 2 g of Li$_2$S, P$_2$S$_5$, and LiCl with a stoichiometric ratio of 5:1:2

was employed. The raw materials were manually mixed for 10 min prior to introduction into 45 mL zirconia pots with zirconia balls (10 mm, 10 balls). A rotation speed of 600 rpm and a rotation time of 20 h were employed.

XRD patterns were recorded using Bruker X8 with a CuK_{α} radiation. The samples were covered with amorphous Kapton film because of their hygroscopic properties.

The total resistivity of the prepared samples was investigated using AC impedance spectroscopy, as reported previously [26]. DC conduction was recorded using stainless steel (SUS) rods as blocking electrodes and lithium metal sheets as non-blocking electrodes. Prior to the measurements, the sample $(80Li_2S - 20AlI_3) \cdot 10LiI$ was made into pellets of about 10 mm in diameter (550 MPa, at RT). Since the sample $(80Li_2S - 20AlI_3) \cdot 10LiI$ continuously reacts with Li metal, a thin layer of Li_6PS_5Cl solid electrolyte was introduced to the cell to prevent $(80Li_2S - 20AlI_3) \cdot 10LiI$ from direct contact with Li metal. Two SUS rods were employed as current collectors. The currents were measured using a potentiostat (PGSTAT302N, Autolab, Herisau, Switzerland) with applied voltages of 0.2–0.7 V (DC) for 60 min.

DC polarization curves were recorded using the cell Li|Li_6PS_5Cl|$(80Li_2S - 20AlI_3)\cdot$ 10LiI|Li_6PS_5Cl|Li cycling at ± 0.05, ± 0.1, and ± 0.2 mA cm^{-1} [27].

Two-step planetary ball milling was used to prepare the composite cathode. In total, 0.3 g of CuS and Ketjen Black (weight ratio of 4:1) were mixed in zirconia pots using 30 g of zirconia balls (4 mm) at 410 rpm for 10 h. Then, 0.2 g of $(80Li_2S - 20AlI_3)\cdot 10LiI$ was added, and the positive electrode composites were obtained after 2 h mixing at 300 rpm. The ASS Li-S cell was constructed as previously reported using the prepared electrode composite, Li_6PS_5Cl, and $Li_{4.4}Si$ [26]. The cells were cycles using either CC or CC-CV mode to study the stability of $(80Li_2S - 20AlI_3)\cdot 10LiI$ at a high voltage range. The current density was 0.25 mA cm^{-2}.

All the experiments were carried out in a glove box (Ar-filled, [H_2O] < 0.1 ppm) or an airtight sample holder.

3. Results and Discussion

Figure 1 shows the XRD patterns of $(100 - x)Li_2S$-xAlI_3 (Figure 1a) and $(80Li_2S - 20AlI_3)\cdot yLiI$ (Figure 1b) composite solid electrolytes (y = 5, 10, 15). Sample Li_2S (x = 0) was characterized by four intense peaks located at $2\theta \approx 27.03$, 31.22, 44.77, and 53.15°. The pattern of AlI_3 (x = 100) has two intense peaks at $2\theta \approx 25.24$ and 29.06°. Samples x = 7 and x = 10 exhibited characteristic peaks of both Li_2S and AlI_3; however, the features of AlI_3 were more clearly observed in sample x = 10 than in sample x = 7. The features of Li_2S disappeared in the samples x = 20, 25, and 30, indicating that Li_2S became amorphous or a new crystal structure was formed because the XRD pattern of those samples did not completely cover AlI_3 peaks. It was also proved that samples $5 \geq x \geq 0$ exhibited the crystal structure of Li_2S [23]. Therefore, $(100 - x)Li_2S$-xAlI_3 exhibits the structure of Li_2S when $5 \geq x \geq 0$ and the structure of AlI_3 when $x \geq 20$; those results also show that the $(100 - x)Li_2S$-xAlI_3 solid solution can be prepared by mechanochemical synthesis, and its structure depends on the Li_2S mass fraction. XRD patterns of $(80Li_2S - 20AlI_3)\cdot yLiI$ composites and raw materials are illustrated in Figure 1b. The $(80Li_2S - 20AlI_3)\cdot yLiI$ composites exhibited the characteristic peaks of AlI_3 and no trace of LiI (y = 100) was detected. However, fitting the pattern of sample y = 15 disclosed that the peak at 25.4° is composed of two peaks at 25.4 and 25.9°, and the peak at 29.4° is composed of two peaks at 29.4 and 30.2° (Figure 1c,d). Those fitting results proved that LiI crystal still remained in sample y = 15, while its existence in y = 5 and 10 was not detected. Therefore, LiI might form a solid solution with $80Li_2S - 20AlI_3$ or it exists in the amorphous form in samples y = 5 and 10.
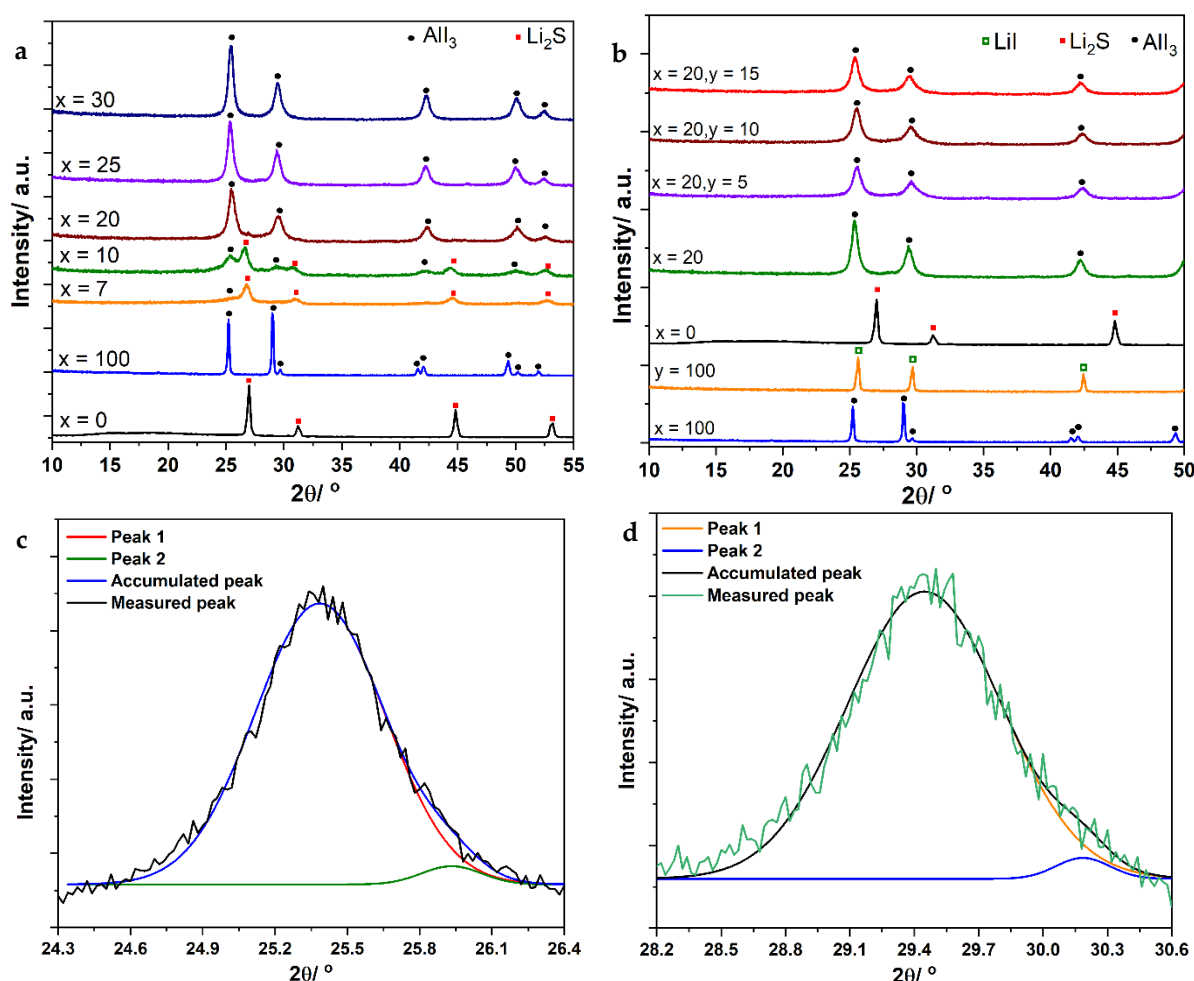
Figure 1. XRD patterns of the prepared samples. (**a**) XRD patterns of $(100 - x)Li_2S\text{-}xAlI_3$; (**b**) XRD patterns of $(80Li_2S - 20AlI_3)\cdot yLiI$ (y = 0, 5, 10, 15); (**c**,**d**) Fitting result of peak at 25.4° and 29.4° of sample y = 15, respectively.

Figure 2 shows the temperature dependence of the ionic conductivity of $(100 - x)Li_2S\text{-}xAlI_3$ (Figure 2a) and $(80Li_2S - 20AlI_3)\cdot yLiI$ (Figure 2b) composite solid electrolytes (y = 5, 10, 15). The small insets show the activation energy of the samples. The ionic conductivity of Li_2S at 25 °C was about 10^{-12} Scm^{-1} [18,23]. Sample x = 7 exhibited ionic conductivity at 25 °C of about 2.8×10^{-5} Scm^{-1}. Samples x = 20, 25, and 20 had ionic conductivity at 25 °C of about 5.8×10^{-5} Scm^{-1}, 3.8×10^{-5} Scm^{-1}, and 3.1×10^{-5} Scm^{-1}, respectively. The activation energy of sample x = 5, 7, 20, 25, and 30 was about 56, 44, 38, 37, and 60 kJ mol^{-1}. The activation energy of the samples decreased when x increased and reached the minima values of about 38 kJ mol^{-1} in samples x = 20, 25. Thus, forming a solid solution with AlI_3 could enhance the ionic conductivity of Li_2S, but the ionic conductivity of $(100 - x)Li_2S\text{-}xAlI_3$ at 25 °C was still lower than 10^{-4} Scm^{-1}. It was reported that the ionic conductivity of Li_3PS_4 improved with LiI addition, so LiI was also added to $80Li_2S - 20AlI_3$ to investigate the ionic conductivity improvement [28,29]. The temperature dependence of the ionic conductivity of $(80Li_2S - 20AlI_3)\cdot yLiI$ composite solid electrolytes (y = 0, 5, 10, 15) are shown in Figure 2b. The conductivity of $80Li_2S - 20AlI_3$ (x = 20, y = 0) at 25 °C was about 5.8×10^{-5} Scm^{-1}; this value increased to 1.1×10^{-4}, 2.3×10^{-4}, and 1.0×10^{-4} Scm^{-1}. The activation energy for the Li-ion movement was about 38, 40, 42, and 42 in samples y = 0, 5, 10, and 15, respectively. The existence of LiI crystals, as shown in Figure 1c,d, is responsible for the decrease in conductivity of sample y = 15 compared with sample y = 10. Thus, LiI addition could enhance the ionic conductivity of $80Li_2S - 20AlI_3$ and

$(80Li_2S - 20AlI_3)\cdot10LiI$ had the highest Li-ion conductivity among the prepared sample at 25 °C.
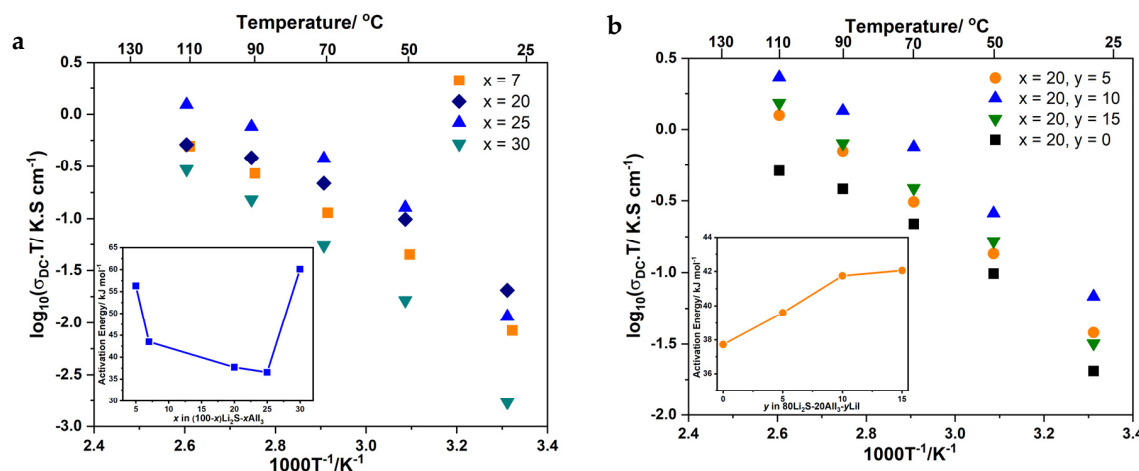
Figure 2. Ionic conductivity of the prepared samples. (**a**) Temperature dependence of ionic conductivity of $(100 - x)Li_2S$-$xAlI_3$ samples and the activation energy (small inset); (**b**) Temperature dependence of ionic conductivity of $(80Li_2S - 20AlI_3)\cdot yLiI$ (y = 0, 5, 10, 15) samples and the activation energy (small inset).

Figure 3a shows the time dependence of DC current when a voltage of 0.2, 0.5, and 0.7 V (DC) was applied to sample $(80Li_2S - 20AlI_3)\cdot10LiI$ using a blocking electrode. The polarization was initially observed, and then the current became nearly constant. The electronic conductivity was about 1.1×10^{-8} Scm^{-1}. Since $(80Li_2S - 20AlI_3)\cdot10LiI$ reacts with Li metal, a thin layer of Li_6PS_5Cl was employed to prevent $(80Li_2S - 20AlI_3)\cdot10LiI$ from direct contact with Li metal. A constant current was obtained when 0.5 V (DC) was applied to the cell $Li|Li_6PS_5Cl|(80Li_2S - 20AlI_3)\cdot10LiI| Li_6PS_5Cl|Li$ (Figure 3b). The constant current obtained using the non-blocking electrode was about 10^4 times higher than that obtained using the blocking electrode; thus, $(80Li_2S - 20AlI_3)\cdot10LiI$ is considered a pure Li-ion conductor with a Li-ion transport number higher than 0.999. In addition, the ionic conductivity calculated from the current values was about 2.1×10^{-4} Scm^{-1} at 25 °C, which resembled the value 2.3×10^{-4} Scm^{-1} obtained from AC impedance spectroscopy.
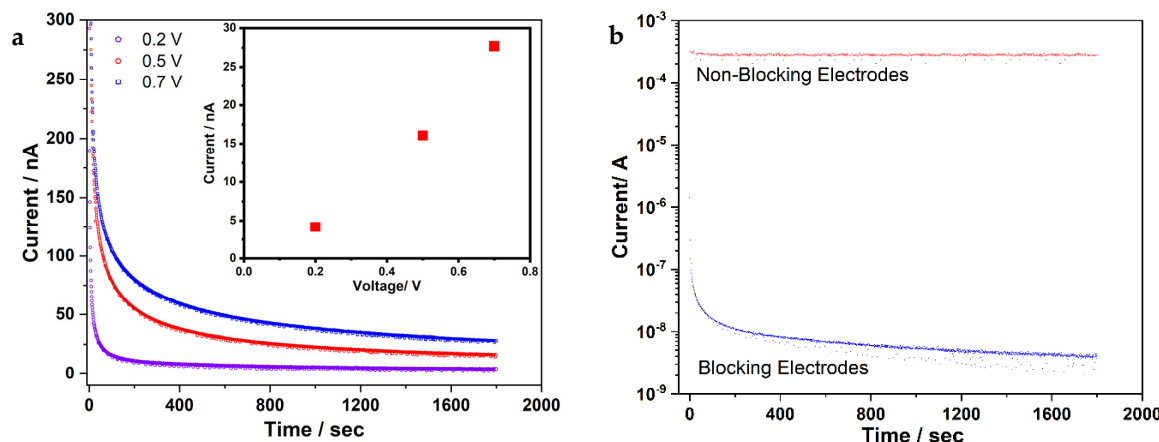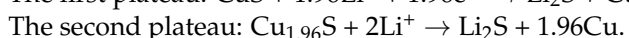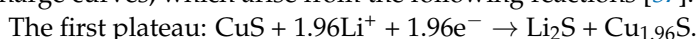
Figure 3. Conductivity of $(80Li_2S - 20AlI_3)\cdot10LiI$. (**a**) Time dependence of the conductivity at constant applied voltage of 0.2, 0.5, and 0.7 V using blocking electrodes $(SUS|(80Li_2S - 20AlI_3)\cdot10LiI|SUS)$; the small inset illustrates the values of constant current at each applied voltage. (**b**) Time dependence of the conductivity at constant applied voltage of 0.5 V using blocking electrodes $(SUS|(80Li_2S - 20AlI_3)\cdot10LiI|SUS)$ and non-blocking electrodes $Li|Li_6PS_5Cl|(80Li_2S - 20AlI_3)\cdot10LiI|Li_6PS_5Cl|Li$.

Figure 4a,b shows the Nyquist plots of $80Li_2S - 20AlI_3$ and $(80Li_2S - 20AlI_3)\cdot10LiI$ measured at 28–90 °C, respectively. All the plots consist of a semicircle and a low-frequency tail, which is consistent with Li^+ blocking at the SUS electrodes, expressing ionic conductive behavior. The diameter of the semicircle gradually decreased with increasing temperature and was almost negligible at 90 °C. The total impedance value of the electrolyte pellet is the value at the intersection point between the semicircle and the x-axis in the intermediate frequency region [30]. The impedance spectra recorded at room temperature of $80Li_2S - 20AlI_3$ and $(80Li_2S - 20AlI_3)\cdot10LiI$ are plotted in Figure 4c,d, respectively. The equivalence circuit of the impedance spectrum is shown in Figure 4c. The impedance resistance of $80Li_2S - 20AlI_3$ is composed of bulk, interface, and grain boundary resistances (the color-filled regions) [31,32]. The bulk resistance of the SE (R_{bulk}) is obtained from the intersection between the semicircle and the x-axis in the high-frequency region. The semicircle in the intermediate region is composed of interfacial resistance ($R_{Interfacial}$) and grain boundary resistance ($R_{Grain\ boundary}$). The R_{bulk} value of $80Li_2S - 20AlI_3$ is close to that of $(80Li_2S - 20AlI_3)\cdot10LiI$. While the $R_{Interfacial} + R_{Grain\ boundary}$ value of $(80Li_2S - 20AlI_3)\cdot10LiI$ is smaller than that of $80Li_2S - 20AlI_3$. These results indicate that LiI addition effectively reduces the value of $R_{Interfacial} + R_{Grain\ boundary}$.

The conductivity isotherms of $80Li_2S - 20AlI_3$ and $(80Li_2S - 20AlI_3)\cdot10LiI$ recorded from 28 to 90 °C, the real part σ′ of the complex conductivity plotted against frequency F, are depicted in Figure 4e,f, respectively. The isotherms display a frequency independence plateau in high and intermediate frequency regions, which is the so-called direct current (DC) region [33,34]. This region indicates long-range ion transport. Frequency dependence of conductivity is clearly observed in the low-frequency region, which exhibits the polarization effect. Jonscher's power law $σ′ \propto ω^n$ was observed in the low-frequency region, where $ω$ is the angular frequency and n represents the interaction between the mobile ion and its surrounding environment [35,36]. Temperature dependence of n is clearly observed in sample $80Li_2S - 20AlI_3$ and the n values are higher than 0.6, indicating the dipole behaviors of charge carriers in this sample [36]. Two distinct slopes appear in the low-frequency region of the isotherms of sample $(80Li_2S - 20AlI_3)\cdot10LiI$, with n values close to 0.7 and 0.5. The n values also indicated the dipoles behaviors of charge carriers, but the presence of two slopes suggested the existence of two types of materials in the sample $(80Li_2S - 20AlI_3)\cdot10LiI$.

$LiI(80Li_2S - 20AlI_3)\cdot10LiI||Li$ and $Li|Li_6PS_5Cl|(80Li_2S - 20AlI_3)\cdot10LiI|Li_6PS_5Cl|Li$ symmetric cells were employed to investigate the stability of $(80Li_2S - 20AlI_3)\cdot10LiI$ at a low voltage region. The small inset in Figure 5a proved that the reaction between $(80Li_2S - 20AlI_3)\cdot10LiI$ and Li metal is irreversible. However, the $Li|Li_6PS_5Cl|(80Li_2S - 20AlI_3)\cdot10LiI|Li_6PS_5Cl|Li$ symmetric cell exhibited a relatively steady charge–discharge voltage for more than 200 h. These results indicated that $(80Li_2S - 20AlI_3)\cdot10LiI$ irreversibly reacts with Li metal, but it is quite stable in the low-voltage region. All-solid-state cells, which employed $(80Li_2S - 20AlI_3)\cdot10LiI$, as solid electrolyte in the positive electrode, were fabricated to study their stability at high voltage regions. CuS and $Li_{4.4}Si$ were used as active materials. Figure 5b–e illustrates the electrochemical performances of the prepared cells. The 1st and 10th charge—discharge curves of the cells cycling using CC and CC-CV modes are depicted in Figure 5b,d, respectively. Two distinct plateaus are observed in the discharge curves, which arise from the following reactions [37]:

The first plateau: $CuS + 1.96Li^+ + 1.96e^- \rightarrow Li_2S + Cu_{1.96}S$.
The second plateau: $Cu_{1.96}S + 2Li^+ \rightarrow Li_2S + 1.96Cu$.

Accordingly, two distinct plateaus also appeared in the charge curves. The charge curve in Figure 5b was smooth at low voltage and bumpy at voltage higher than 2.3 V, which illustrated the decomposition of $(80Li_2S - 20AlI_3)\cdot10LiI$ composite solid electrolyte. The discharge and charge capacity were about 400 and 600 mAh g^{-1}_{CuS}, respectively (Figure 5c), resulting in the capacity loss of about 200 mAh g^{-1}_{CuS} and unstable Coulombic efficiency (Figure 5c). Figure 5c indicates that the discharge capacity was stable at about 400 mAh g^{-1}_{CuS} but the charge capacity was unsteady, showing the continuous

decomposition of solid electrolyte. The cyclic voltammogram of Li_3SI solid electrolyte also indicated the oxidation of S^{2-} at about 2 V, which was one of the reasons for low capacity retention of the all-solid-state cell cycling in the voltage range of 2.0–3.6 V [24]. Thus, $(80Li_2S - 20AlI_3)·10LiI$ composite solid electrolyte was irreversibly decomposed at voltage higher than 2.3 V. The cell cycling in CC-CV mode (CC: 0.25 mA cm^{-2}, CV: 2.30 V) exhibits smooth charge–discharge curves (Figure 5d), confirming that $(80Li_2S - 20AlI_3)·10LiI$ was stable in this voltage region. The charge–discharge capacity was stable at about 400 mAh g^{-1}_{CuS}, resulting in a Coulombic efficiency higher than 99.5%.
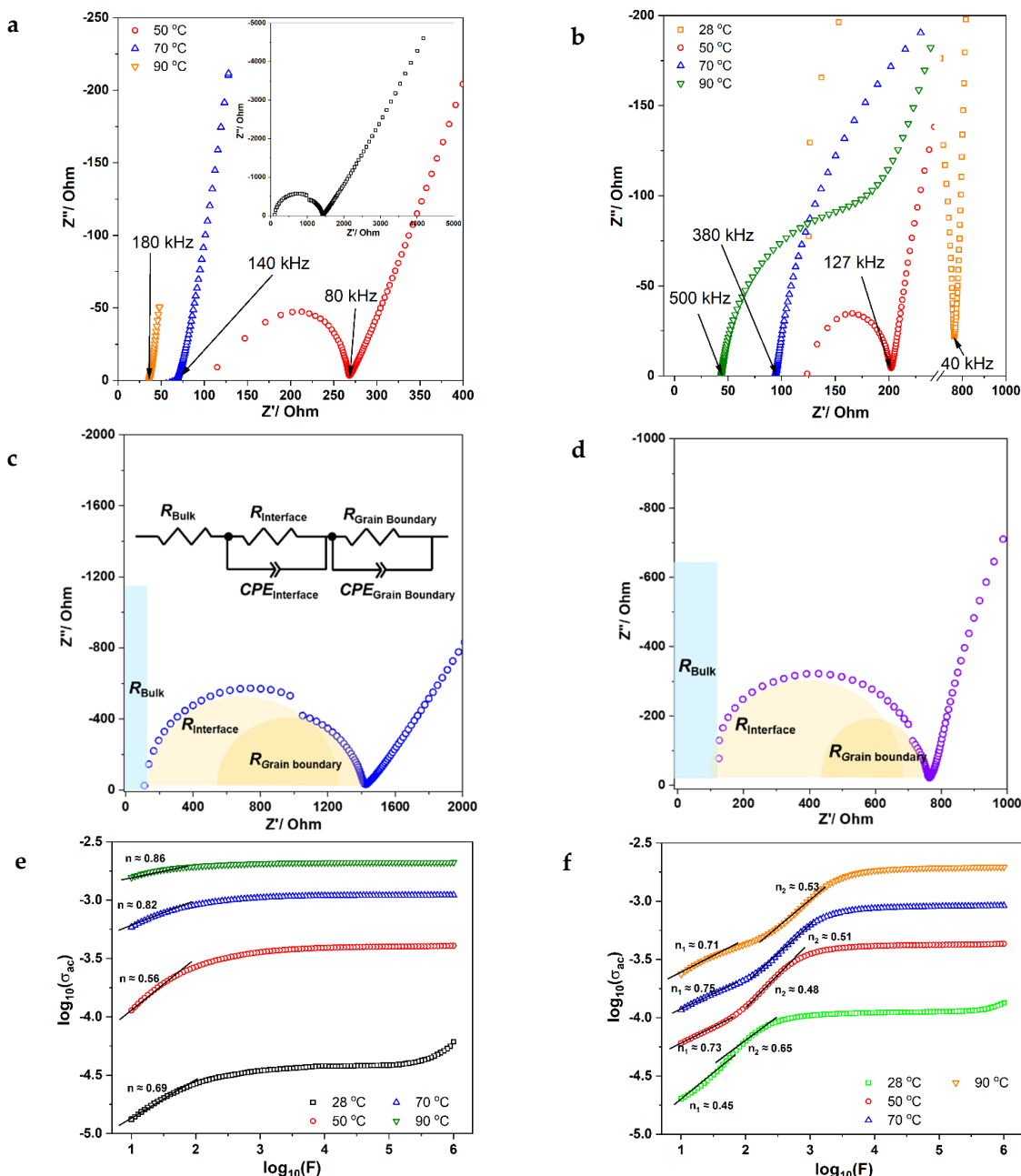
Figure 4. (**a**) Nyquist plots of $80Li_2S - 20AlI_3$ measured from 28 to 90 °C (the inset shows the Nyquist plot at 28 °C); (**b**) Nyquist plots of $(80Li_2S - 20AlI_3)·10LiI$ measured from 28 to 90 °C; (**c**,**d**) the matching impedance figures, equivalent circuit of $80Li_2S - 20AlI_3$ and $(80Li_2S - 20AlI_3)·10LiI$ measured at 28 °C, respectively; (**e**) conductivity isotherms (10 Hz to 1 MHz) of $80Li_2S - 20AlI_3$ measured from 28 to 90 °C; (**f**) conductivity isotherms (10 Hz to 1 MHz) of $(80Li_2S - 20AlI_3)·5LiI$ measured from 28 to 90 °C.
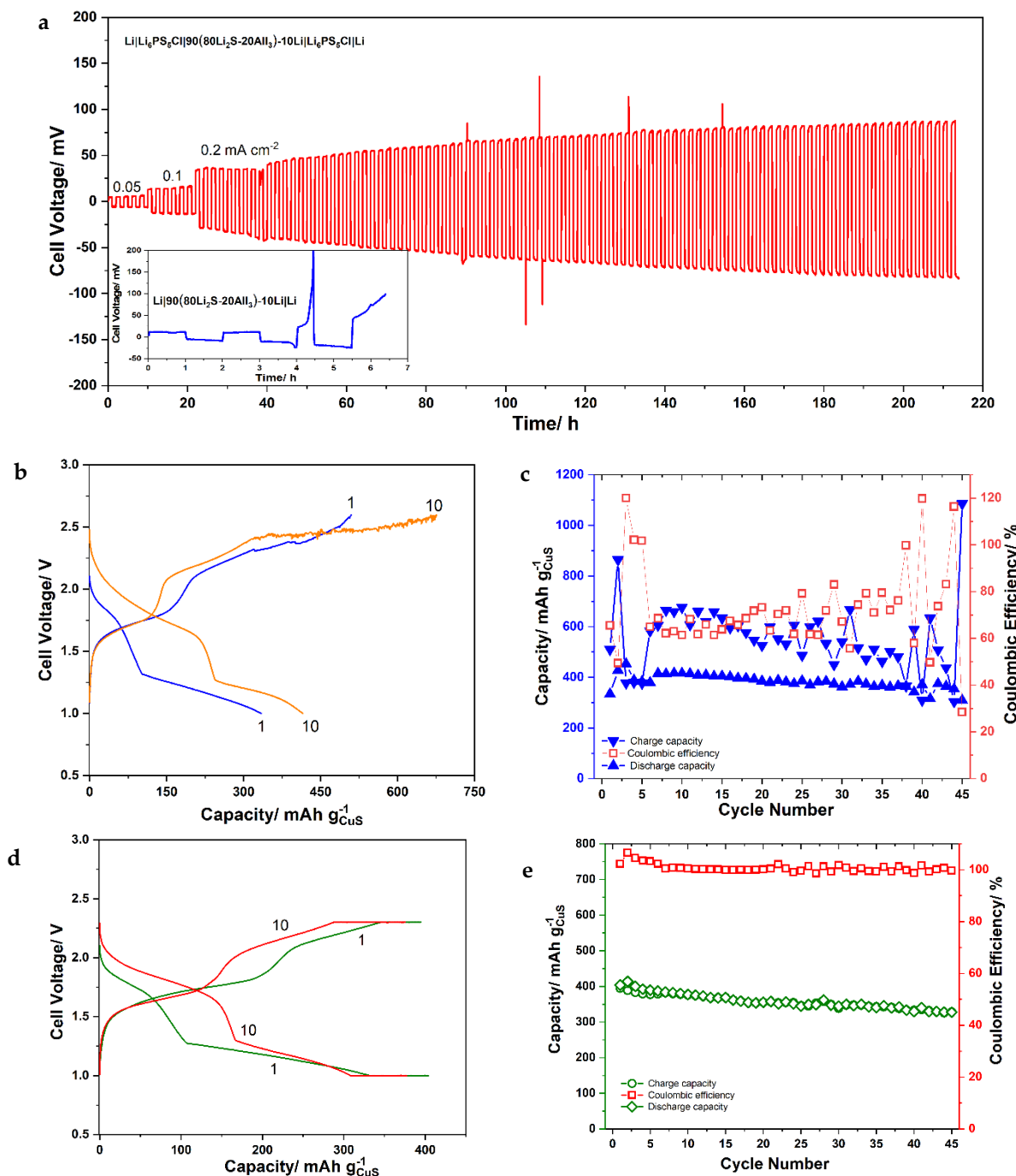
Figure 5. (**a**) Cyclability of the symmetric Li|Li$_6$PS$_5$Cl|(80Li$_2$S − 20AlI$_3$)·10LiI|Li$_6$PS$_5$Cl|Li and Li|(80Li$_2$S − 20AlI$_3$)·10LiI|Li (small inset); (**b**) 1st and 10th charge–discharge curves of the solid-state cell cycled using CC mode; (**c**) cyclic properties of the solid-state cell using CC mode; (**d**) 1st and 10th charge–discharge curves of the solid-state cell cycled using CC-CV mode; (**e**) cyclic properties of the solid-state cell using CC-CV mode.

4. Conclusions

(100 − x)Li$_2$S-xAlI$_3$ and (80Li$_2$S − 20AlI$_3$)·yLiI (y = 0, 5, 10, 15) composite solid electrolytes were successfully prepared by mechanochemical synthesis. XRD results revealed that Li$_2$S and AlI$_3$ formed a solid solution, while LiI crystals remained in sample y = 15. It was also proved that (80Li$_2$S − 20AlI$_3$)·10LiI is a pure Li-ion conductor with the ionic conductivity of about 2.3×10^{-4} Scm^{-1} at 25 °C, about three times higher than that of the

$80Li_2S - 20AlI_3$ sample. The impedance spectroscopy results revealed that LiI addition enhanced the grain boundary and interfacial resistance of the prepared samples. The results from XRD and AC impedance suggested that LiI might be present in the amorphous form in samples y = 5 and 10. The symmetric and all-solid-state cell performance illustrated that $(80Li_2S - 20AlI_3)\cdot 10LiI$ was relatively stable at voltage lower than 2.3 V.

References

1. Zhang, Q.; Cao, D.; Ma, Y.; Natan, A.; Aurora, P.; Zhu, H. Sulfide-Based Solid-State Electrolytes: Synthesis, Stability, and Potential for All-Solid-State Batteries. *Adv. Mater.* **2019**, *31*, e1901131. [CrossRef] [PubMed]
2. Bachman, J.C.; Muy, S.; Grimaud, A.; Chang, H.H.; Pour, N.; Lux, S.F.; Paschos, O.; Maglia, F.; Lupart, S.; Lamp, P.; et al. Inorganic Solid-State Electrolytes for Lithium Batteries: Mechanisms and Properties Governing Ion Conduction. *Chem. Rev.* **2016**, *116*, 140–162. [CrossRef] [PubMed]
3. Chen, S.; Xie, D.; Liu, G.; Mwizerwa, J.P.; Zhang, Q.; Zhao, Y.; Xu, X.; Yao, X. Sulfide solid electrolytes for all-solid-state lithium batteries: Structure, conductivity, stability and application. *Energy Storage Mater.* **2018**, *14*, 58–74. [CrossRef]
4. Seino, Y.; Ota, T.; Takada, K.; Hayashi, A.; Tatsumisago, M. A sulphide lithium super ion conductor is superior to liquid ion conductors for use in rechargeable batteries. *Energy Environ. Sci.* **2014**, *7*, 627–631. [CrossRef]
5. Kamaya, N.; Homma, K.; Yamakawa, Y.; Hirayama, M.; Kanno, R.; Yonemura, M.; Kamiyama, T.; Kato, Y.; Hama, S.; Kawamoto, K.; et al. A lithium superionic conductor. *Nat. Mater.* **2011**, *10*, 682–686. [CrossRef]
6. Adeli, P.; Bazak, J.D.; Park, K.H.; Kochetkov, I.; Huq, A.; Goward, G.R.; Nazar, L.F. Boosting Solid-State Diffusivity and Conductivity in Lithium Superionic Argyrodites by Halide Substitution. *Angew. Chem.* **2019**, *58*, 8681–8686. [CrossRef]
7. Feng, X.; Chien, P.-H.; Patel, S.; Zheng, J.; Immediato-Scuotto, M.; Xin, Y.; Hung, I.; Gan, Z.; Hu, Y.-Y. Synthesis and characterizations of highly conductive and stable electrolyte $Li_{10}P_3S_{12}I$. *Energy Storage Mater.* **2019**, *22*, 397–401. [CrossRef]
8. Sakuda, A.; Yamauchi, A.; Yubuchi, S.; Kitamura, N.; Idemoto, Y.; Hayashi, A.; Tatsumisago, M. Mechanochemically Prepared $Li_2S-P_2S_5-LiBH_4$ Solid Electrolytes with an Argyrodite Structure. *ACS Omega* **2018**, *3*, 5453–5458. [CrossRef]
9. Liu, Z.; Fu, W.; Payzant, E.A.; Yu, X.; Wu, Z.; Dudney, N.J.; Kiggans, J.; Hong, K.; Rondinone, A.J.; Liang, C. Anomalous high ionic conductivity of nanoporous beta-Li_3PS_4. *J. Am. Chem. Soc.* **2013**, *135*, 975–978. [CrossRef]
10. Hayashi, A.; Fukuda, T.; Hama, S.; Yamashita, H.; Morimoto, H.; Minami, T.; Tatsumisago, M. Lithium ion conducting glasses and glass-ceramics in the system $Li_2S-M_xS_y$ (M = Al, Si and P) prepared by mechanical milling. *J. Ceram. Soc. Jpn.* **2004**, *112*, S695–S699.
11. Kondo, S.; Takada, K.; Yamamura, Y. New lithium ion conductors based on Li_2S-SiS_2 system. *Solid State Ionics* **1992**, *53–56*, 1183–1186. [CrossRef]
12. Takada, K.; Aotani, N.; Kondo, S. Electrochemical behaviors of Li+ ion conductor, $Li_3PO_4-Li_2S-SiS_2$. *J. Power Sources* **1993**, *43–44*, 135–141. [CrossRef]
13. Hayashi, A.; Fukuda, T.; Morimoto, H.; Minami, T.; Tatsumisago, M. Amorphous solid electrolytes in the system $Li_2S-Al_2S_3-SiS_2$ prepared by mechanical milling. *J. Mater. Sci.* **2004**, *39*, 5125–5127. [CrossRef]
14. Kinoshita, S.; Okuda, K.; Machida, N.; Naito, M.; Sigematsu, T. All-solid-state lithium battery with sulfur/carbon composites as positive electrode materials. *Solid State Ion.* **2014**, *256*, 97–102. [CrossRef]
15. Seh, Z.W.; Wang, H.; Hsu, P.-C.; Zhang, Q.; Li, W.; Zheng, G.; Yao, H.; Cui, Y. Facile synthesis of Li_2S–polypyrrole composite structures for high-performance Li_2S cathodes. *Energy Environ. Sci.* **2014**, *7*, 672. [CrossRef]
16. Wu, F.; Magasinski, A.; Yushin, G. Nanoporous Li_2S and MWCNT-linked Li_2S powder cathodes for lithium-sulfur and lithium-ion battery chemistries. *J. Mater. Chem. A* **2014**, *2*, 6064–6070. [CrossRef]
17. Han, F.; Yue, J.; Fan, X.; Gao, T.; Luo, C.; Ma, Z.; Suo, L.; Wang, C. High-Performance All-Solid-State Lithium-Sulfur Battery Enabled by a Mixed-Conductive Li_2S Nanocomposite. *Nano Lett.* **2016**, *16*, 4521–4527. [CrossRef]
18. Lin, Z.; Liu, Z.; Dudney, N.J.; Liang, C. Lithium Superionic Sulfide Cathode for All-Solid Lithium-Sulfur Batteries. *ACS Nano* **2013**, *7*, 2829–2833. [CrossRef]

19. Jiang, H.; Han, Y.; Wang, H.; Zhu, Y.; Guo, Q.; Jiang, H.; Zheng, C.; Xie, K. Li_2S-Li_3PS_4 (LPS) Composite Synthesized by Liquid-Phase Shaking for All-Solid-State Lithium-Sulfur Batteries with High Performance. *Energy Technol.* **2020**, *8*, 2000023. [CrossRef]

20. Hakari, T.; Hayashi, A.; Tatsumisago, M. Li_2S-Based Solid Solutions as Positive Electrodes with Full Utilization and Superlong Cycle Life in All-Solid-State Li/S Batteries. *Adv. Sustain. Syst.* **2017**, *1*, 1700017. [CrossRef]

21. Phuc, N.H.H.; Takaki, M.; Kazuhiro, H.; Hiroyuki, M.; Atsunori, M. Dual effect of MgS addition on Li_2S ionic conductivity and all-solid-state Li–S cell performance. *SN Appl. Sci.* **2020**, *2*, 1803. [CrossRef]

22. Phuc, N.H.H.; Takaki, M.; Hiroyuki, M.; Atsunori, M. Preparation of $Li_{2-3x}Al_xS$ for All-Solid-State Li-S Battery. *Front. Energy Res.* **2021**, *8*, 606023. [CrossRef]

23. Gamo, H.; Maeda, T.; Hikima, K.; Deguchi, M.; Fujita, Y.; Kawasaki, Y.; Sakuda, A.; Muto, H.; Phuc, N.H.H.; Hayashi, A.; et al. Synthesis of an AlI_3-doped Li_2S positive electrode with superior performance in all-solid-state batteries. *Mater. Adv.* **2022**, *3*, 2488–2494. [CrossRef]

24. Rajagopal, R.; Park, M.-H.; Subramanian, Y.; Jung, Y.J.; Ryu, K.-S. Synthesis and electrochemical performance of antiperovskite-like Li_3SI solid electrolyte. *J. Electroanal. Chem.* **2021**, *895*, 115477. [CrossRef]

25. Tamori, R.; Machida, N.; Shigematsu, T. Preparation of $Li_{4.4}Si$ Alloy by Use of Mechanical Milling Methods and Its Properties as Negative Electrodes in Lithium Cells. *J. Jpn. Soc. Powder Powder Metall.* **2001**, *48*, 267–273. [CrossRef]

26. Phuc, N.H.H.; Gamo, H.; Hikima, K.; Muto, H.; Matsuda, A. Novel $(100-x-y)Li_3PS_4$-$xLiBF_4$-$yLiCl$ amorphous solid electrolytes for all-solid-state Li ion battery. *J. Non-Cryst. Solids* **2022**, *593*, 121768. [CrossRef]

27. Phuc, N.H.H.; Maeda, T.; Yamamoto, T.; Muto, H.; Matsuda, A. Preparation of Li_3PS_4–Li_3PO_4 Solid Electrolytes by Liquid-Phase Shaking for All-Solid-State Batteries. *Electron. Mater.* **2021**, *2*, 39–48. [CrossRef]

28. Suyama, M.; Kato, A.; Sakuda, A.; Hayashi, A.; Tatsumisago, M. Lithium dissolution/deposition behavior with Li_3PS_4-LiI electrolyte for all-solid-state batteries operating at high temperatures. *Electrochim. Acta* **2018**, *286*, 158–162. [CrossRef]

29. Rangasamy, E.; Liu, Z.; Gobet, M.; Pilar, K.; Sahu, G.; Zhou, W.; Wu, H.; Greenbaum, S.; Liang, C. An iodide-based $Li_7P_2S_8I$ superionic conductor. *J. Am. Chem. Soc.* **2015**, *137*, 1384–1387. [CrossRef]

30. Suzuki, K.; Sakuma, M.; Hori, S.; Nakazawa, T.; Nagao, M.; Yonemura, M.; Hirayama, M.; Kanno, R. Synthesis, structure, and electrochemical properties of crystalline Li–P–S–O solid electrolytes: Novel lithium-conducting oxysulfides of $Li_{10}GeP_2S_{12}$ family. *Solid State Ion.* **2016**, *288*, 229–234. [CrossRef]

31. Xu, R.C.; Xia, X.H.; Yao, Z.J.; Wang, X.L.; Gu, C.D.; Tu, J.P. Preparation of $Li_7P_3S_{11}$ glass-ceramic electrolyte by dissolution-evaporation method for all-solid-state lithium ion batteries. *Electrochim. Acta* **2016**, *219*, 235–240. [CrossRef]

32. Wei, J.; Kim, H.; Lee, D.-C.; Hu, R.; Wu, F.; Zhao, H.; Alamgir, F.M.; Yushin, G. Influence of annealing on ionic transfer and storage stability of Li_2S–P_2S_5 solid electrolyte. *J. Power Sources* **2015**, *294*, 494–500. [CrossRef]

33. Gombotz, M.; Wilkening, H.M.R. Fast Li Ion Dynamics in the Mechanosynthesized Nanostructured Form of the Solid Electrolyte Li_3YBr_6. *ACS Sustain. Chem. Eng.* **2020**, *9*, 743–755. [CrossRef]

34. Hanghofer, I.; Brinek, M.; Eisbacher, S.L.; Bitschnau, B.; Volck, M.; Hennige, V.; Hanzu, I.; Rettenwander, D.; Wilkening, H.M.R. Substitutional disorder: Structure and ion dynamics of the argyrodites Li_6PS_5Cl, Li_6PS_5Br and Li_6PS_5I. *Phys. Chem. Chem. Phys. PCCP* **2019**, *21*, 8489–8507. [CrossRef]

35. Jonscher, A.K. The 'universal' dielectric respond. *Nature* **1977**, *267*, 673–679. [CrossRef]

36. Ngai, K.L.; Jonscher, A.K.; White, C.T. On the origin of the universal dielectric respond in condensed matter. *Nature* **1979**, *277*, 185–189. [CrossRef]

37. Hayashi, A.; Ohtomo, T.; Mizuno, F.; Tadanaga, K.; Tatsumisago, M. All-solid-state Li S batteries with highly conductive glass–ceramic electrolytes. *Electrochem. Commun.* **2003**, *5*, 701–705. [CrossRef]